Non-Saturated 3E (Energy, Exergy, and Economic) Analysis of Carnot Battery Systems Based on Organic Rankine Cycle

Ruiqiang Ma and Bin Yang*

Tianjin Key Laboratory of Clean Energy and Pollution Control, School of Energy and Environment Engineering, Hebei University of Technology, Tianjin 300401, PR China

ARTICLE INFO

ABSTRACT

Artificial activities, environmental factors, and industrial production lead to periodic fluctuations in electricity consumption, necessitating peak-shaving measures to ensure efficient and stable operation of the power grid. The Carnot battery system represents an effective solution due to its high efficiency and convenience. In this paper, we propose a novel Carnot battery system based on a dual-function unit and establish thermodynamic and economic models. This paper proposed a simple reversible heat pump-organic Rankine cycle Carnot battery system, where a compression and expansion dual-function unit was developed to simplify the system and reduce investment costs. Subsequently, considering the unsaturated operating conditions that occur during practical operation, a comprehensive performance analysis of the system is conducted by varying pressure and temperature parameters. Afterward, an exergy analysis is performed on the proposed system to determine the exergy losses of its components for subsequent optimization. The results indicate that pressure drop has a detrimental effect on the system. When the pressure drop is 15 kPa, the system achieves a power-to-power ratio (P2P), levelized cost of storage (LCOS), and exergy efficiency of 27.57%, 0.66 \$/kW·h, and 62.8%. However, this also leads to increased exergy losses in the evaporator, resulting in decreased exergy efficiency. The evaporator exhibits the highest exergy loss, with a maximum loss of 21.16 kW among all components. Undercharging mode, the condenser shows the lowest exergy efficiency of 64.43%.

*Corresponding Author
Email: yangbin0720@hebut.edu.cn

1. Introduction

The power grid experiences peak demand periods due to factors such as industrial production and human activities. However, excessive load during these peak periods can lead to a series of issues, including inadequate power supply, increased electricity costs, and potential electrical safety hazards [1]. Peak shaving in the power grid refers to the ability of the grid to balance power supply and demand by implementing measures during periods of high demand. Peak shaving ensures stable operation of the power grid, mitigates the risk of power supply shortages or surpluses, and enables the power system to cope with fluctuations in load demand [2]. To achieve a balance between power supply and demand, peak shaving in the power grid can be implemented through various methods [3]: (1) Increasing generation capacity: This involves augmenting the output of power generation equipment, such as operating backup generator units or initiating auxiliary power generation sites, to meet the electricity demand during peak periods; (2) Load adjustment: This entails reducing or delaying the operation of non-critical loads, such as adjustable loads in industrial production, to decrease overall electricity demand; (3) Energy storage systems: This entails utilizing energy storage devices like battery banks or pumped-storage systems to store excess electricity and release it during peak periods, effectively balancing power supply and demand.

Hydroelectric pumped storage, compressed air energy storage, and electrochemical energy storage are widely used forms of energy storage. However, the deployment of the first two methods is challenging due to geographical limitations, while the latter has higher costs during the storage process [4]. Carnot battery, also known as Pumped Thermal Energy Storage (PTES), is a promising technique for electrical energy conversion. It utilizes electricity to extract and store heat, which can then be converted back into electricity when needed [5]. Carnot battery offers several advantages over traditional battery technologies. Firstly, its capacity can be adjusted according to demand without being limited by fixed capacity. Secondly, it achieves high energy density by utilizing temperature differences for energy storage. Additionally, the Carnot battery has lower material costs and better environmental performance due to the use of water as a medium [6]. Carnot batteries can have different structures depending on the specific power cycle. The main power cycles include the Brayton cycle or the Rankine cycle. The Brayton cycle has higher efficiency compared to the Rankine cycle but requires higher storage temperatures (>300℃). However, in practical operation, industrial waste heat and geothermal heat are typically used as low-temperature heat sources, which cannot meet the requirements of the Brayton cycle. The Rankine power cycle, on the other hand, can match low-temperature heat sources, providing stable operation and higher energy density. The combined coupling of a heat pump (HP) and an Organic Rankine Cycle (ORC) forms the Carnot battery [7].

Currently, research on Carnot batteries mainly focuses on improving system performance through changes in system configuration and optimization of operating conditions. Niu *et al*. [8] proposed a new form of Carnot battery by integrating it with a heat storage system and utilizing solar energy and waste heat as heat sources. They compared the Carnot regenerator battery with the basic Carnot battery and concluded that the Carnot regenerator battery using R601fa-R0 as the working fluid is the optimal solution. Canpolat *et al*. [9] presented a novel analysis method for photovoltaic-driven Carnot batteries, conducting a sustainability analysis and combining concepts based on energy and exergy analysis to optimize the Carnot battery system. The results indicate that these different analysis methods are fully applicable to Carnot batteries.

The economic performance is also an essential aspect of evaluating Carnot batteries, as excellent economic performance ensures their wider promotion and application. Hu *et al*. [10] developed an economic model for an integrated Carnot battery system and evaluated the storage costs for 50 scenarios by changing key parameters. They found that costs could increase by 47% when the thermoelectric conversion efficiency improved from 50% to 120%, and the lowest Levelized Cost of Storage (LCOS) was 0.23 $/kW·h. Dai *et al*. [11] established a finite-time thermodynamic model for a Carnot battery system based on the Rankine cycle, analyzing the system with variables such as temperature and area. The analysis results showed that the optimized LCOS was 329.1 $/kW·h at an evaporator temperature of 78°C. With an increase in evaporator temperature, the LCOS decreased by 45.8%. Fan *et al*. [12] developed an energy, exergy, and economic model for the Carnot battery system and optimized the system using genetic algorithms. They discovered that raising the heat storage temperature from 90°C to 130°C

gradually reduced the LCOS from 0.42 $/kW·h to 0.29 $/kW·h. Additionally, they assessed the costs of components, with turbines and compressors representing the largest proportion of total investment.

There have been many studies conducted by scholars on the efficiency and economic aspects of Carnot systems. However, the aforementioned research has generally focused on Carnot systems established under stable and saturated conditions. In this study, we will observe the influence of various factors on system performance when deviating from the saturated state by altering the state of the working fluid. This research will provide a theoretical foundation for the establishment of practical systems.

2. System Description

Fig. (**1**) represents the proposed flowchart of the Carnot cycle. The Carnot energy storage system consists of two parts: the Organic Rankine Cycle (ORC) and the Heat Pump (HP), represented by the red and blue lines, respectively. The working fluid is indicated by the purple line during the system operation. The ORC system and the HP system share a dual-function unit, which can perform expansion and compression processes by changing the direction of operation. The feasibility of the dual-function unit has been extensively studied previously. The Carnot cycle operates in two modes: the discharge mode and the charge mode.

In the discharge mode: valves V3, V4, V7, and V8 are opened, while the other valves are closed. High-temperature water from the hot water tank (H-tank) transfers heat to the ORC system through the evaporator, and after the heat exchange, the high-temperature water is transformed into low-temperature water and stored in the low-temperature water tank (L-tank). The ORC system drives the dual-function unit to expand and generate electricity through the generator, and the cooling capacity is obtained from the cold source in the condenser to ensure the operation of the cycle.

In the charge mode: valves V1, V2, V5, and V6 are opened, while the other valves are closed. The heat source (industrial waste heat, geothermal, etc.) transfers heat to the HP system through the evaporator. The dual-function unit in the HP system undergoes a compression process. Low-temperature water from the L-tank obtains heat through the condenser and is transformed into high-temperature water, which is then stored in the H-tank, completing the charging process.
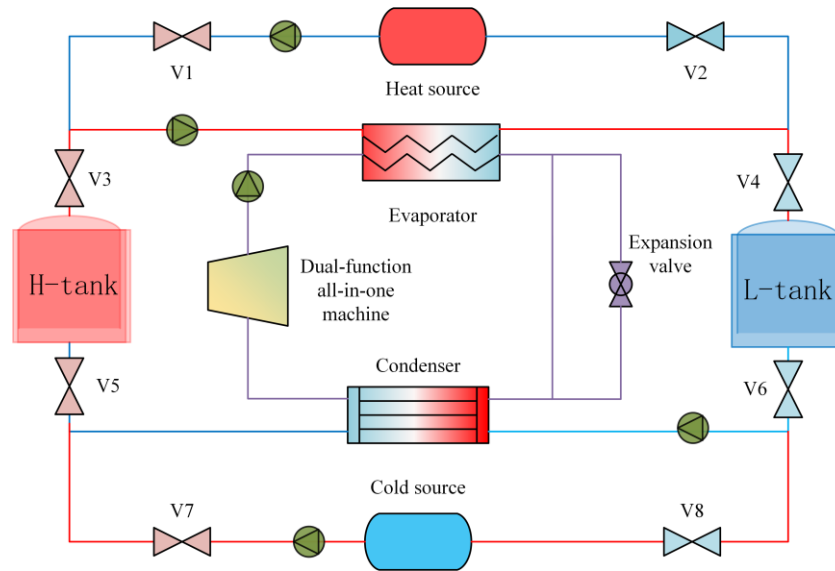

Figure 1: Schematic diagram of Carnot battery system.

3. Mathematical Models

In our previous studies, we have demonstrated that R1233zd(E) can serve as the working fluid for Carnot batteries due to its favorable environmental factors and performance [13]. The specific cycle process is illustrated

in Fig. (**2**). The discharge process operates the ORC system, represented by the blue line in the figure. The charge process operates the HP system, represented by the red line. The variation of the high-temperature thermal storage tank and low-temperature thermal storage tank can be observed through the orange line.
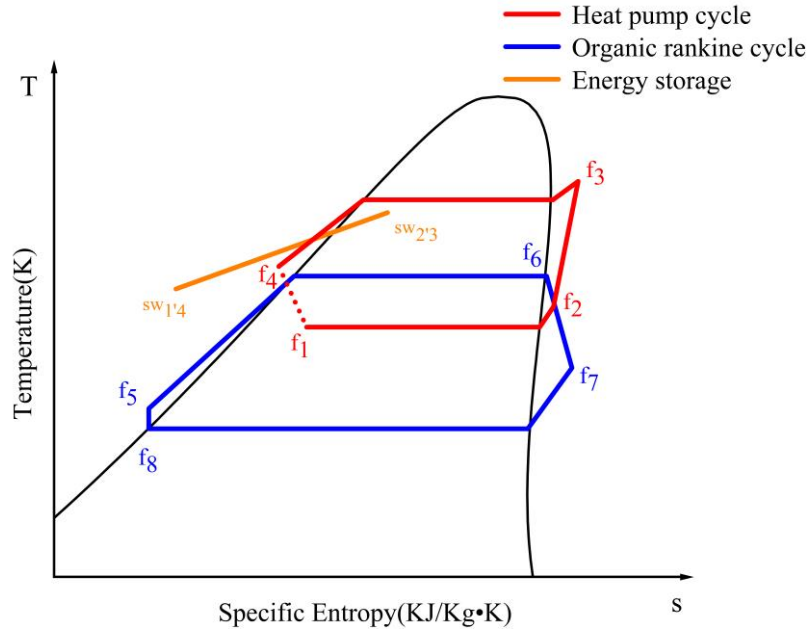

Figure 2: T-s diagram of the Carnot battery system.

The modeling and computational process of the Carnot battery was conducted in MATLAB, and the parameter states were obtained by calling Refprop 10.0. In this study, thermodynamic performance and economic performance models were established. For simplification, the following assumptions were made during the modeling and computational process [14]:

1. Pressure drop and heat losses in pipes and components in the Carnot battery are neglected.

2. The system can operate stably under the specified operating conditions.

3. The isentropic efficiency and heat transfer efficiency of the system remain constant.

4. The throttling process is considered ideal and isentropic.

5. The system is assumed to reach the saturated state at the predetermined conditions in the evaporator and condenser.

3.1. Energy Model

The Cano battery system consists of two modes: discharge mode and charge mode. In the discharge mode, the system operates the ORC system. The heat stored in the high-temperature water tank is converted into electrical energy through the ORC system and released. The efficiency of this thermal-electric conversion process is measured by parameter η_{orc}. The higher the value of η_{orc}, the higher the conversion rate and the better the system performance. It can be calculated using the following equation [15]:

$$\eta_{orc} = \frac{W_{net}}{Q_{s,hp}} = \frac{W_{out} - W_{pump}}{Q_{s,hp}} \tag{1}$$

W_{pump} represents the power consumption of the pump and can be calculated as:

$$P_{pump} = m_f * (h_{f5} - h_{f8}) \tag{2}$$

In this context, W_{net} denotes the net power (KW), while $Q_{s,hp}$ representing the amount of heat stored in the Carnot system.

In charging mode, the system operates an HP system. The low-temperature heat source is converted into high-quality heat via the HP and stored in a high-temperature water tank, with the performance of the HP system assessed using the COP [16]:

$$COP = \frac{Q_{s,hp}}{W_{in}} = \frac{m_{hp} * (h_{f7} - h_{f4})}{m_{hp} * (h_{f7} - h_{f6})} \tag{3}$$

In this case, h represents the enthalpy value at a given state point, and m_{hp} denotes the working fluid flow rate.

The overall thermodynamic efficiency of the Carnot battery system can be assessed using the P2P [17]:

$$P2P = COP\, \eta_{orc}\, \eta_{sto} \tag{4}$$

where, η_{sto} represents the energy storage efficiency, which is assumed as 0.95 [18].

3.2. Exergy Model

Exergy analysis provides a comprehensive assessment of energy systems: Exergy analysis not only considers the efficiency of energy conversion but also takes into account the loss of energy quality. By conducting an Exergy analysis on each component within the system, it is possible to determine which components or processes need improvement or replacement to enhance the overall energy efficiency of the system [19]. In this paper, the thermodynamic efficiency of the Carnot battery system proposed through Exergy efficiency evaluation is assessed. The Exergy efficiency balance equation for each component can be calculated as follows:

$$\sum Ex_{in} + P_{in} = \sum Ex_{out} + P_{out} + L \tag{5}$$

where L is the component exergy loss rate, and P_{in} represents the input power. Ex_i is the exergy rate and can be expressed as follows:

$$Ex_i = m[(h - h_0) - T_0(s - s_0)] \tag{6}$$

where T_0, s_0, h_0 is the reference state.

Exergy balance equations and exergy efficiencies for various components are defined in Table **1**.

Table 1:   The exergy rate equation and exergy equation of component [20, 21].

Component	Exergy Rate Balance Equation	Exergy Efficiency
Evaporator(HP)	$Ex_{hs1} + Ex_{f1} = Ex_{hs2} + Ex_{f_2} + L_{evap,HP}$	$\varphi = (Ex_{f_2} - Ex_{f_1})/(Ex_{hs1} - Ex_{hs2})$
Evaporator(ORC)	$Ex_{sw3} + Ex_{f5} = Ex_{sw4} + Ex_{f_6} + L_{evap,ORC}$	$\varphi = (Ex_{f_6} - Ex_{f_5})/(Ex_{sw3} - Ex_{sw4})$
Condenser (HP)	$Ex_{cs1} + Ex_{sw1} = Ex_{cs2} + Ex_{sw2} + L_{cond,HP}$	$\varphi = (Ex_{sw2} - Ex_{sw1})/(Ex_{f3} - Ex_{f_4})$
Condenser (ORC)	$Ex_{cs1} + Ex_{f7} = Ex_{cs2} + Ex_{f_8} + L_{cond,ORC}$	$\varphi = (Ex_{f_7} - Ex_{f_8})/(Ex_{cs2} - Ex_{cs1})$
Dual-function unit for compressor (HP)	$P_{in} + Ex_{f2} = Ex_{f3} + L_{dfu,HP}$	$\varphi = (Ex_{f3} - Ex_{f2})/P_{in}$
Dual-function unit for expander (ORC)	$Ex_{sw3} = Ex_{sw4} + P_{out} + L_{dfu,ORC}$	$\varphi = (Ex_{sw3} - Ex_{sw4})/P_{out}$
Working fluid Pump	$Ex_{f8} + P_{pump} = Ex_{f5} + L_{pump}$	$\varphi = (Ex_{f5} - Ex_{f8})/P_{pump}$
Throttle valve	$Ex_{f4} = Ex_{f1} + L_{thv}$	$\varphi = Ex_{f1}/Ex_{f4}$

The overall exergy efficiency of the system is calculated as follows:

$$\varphi_t = \frac{P_{out} + E_{hs2} + E_{cs2}}{P_{in} + P_{pump} + E_{hs1} + E_{cs1}} \tag{7}$$

where E_{hs1} is the exergy rate of the heat source unit in the charging mode, denotes the cooling source in the discharging mode. E_{cs1}, E_{cs2} refers to the threshold of the inlet and outlet of the cold source in the discharge mode, respectively. P_{out}, P_{in} represents the output power of system in the discharge mode and the input power of system in the charge mode, respectively. P_{pump} is the power consumption of the pump.

3.3. Economic Model

During the operation of the Carnot battery, economic considerations must be taken into account, as higher economic benefits are conducive to the promotion and application of the Carnot battery. The LCOS represents the cost per unit of electricity storage and has been widely used in storage technologies. The proposed Carnot energy storage battery can use LCOS to measure economic benefits:

$$LCOS = \frac{I_{nvc} + \sum_{i=1}^{n} \frac{A_c}{(1+i)^i}}{\sum_{i=1}^{n} \frac{E_{out}}{(1+i)^i}} \tag{8}$$

where A_c represents the annual operating cost, i denotes the system's service life, which is 20 years [22], and I_{nvc} refers to the initial investment:

$$I_{nvc} = I_{nvc,dfu} + I_{nvc,thv} + I_{nvc,evap} + I_{nvc,cond} + I_{nvc,tank} + I_{nvc,pump} \tag{9}$$

The aforementioned equation describes the initial investment of various components in the system, and the detailed calculation equation is provided in Table **2**.

The heat exchange area (evaporator, condenser) of the heat exchanger can be calculated using the following equation:

$$A = \frac{Q}{KF\Delta T_{lm}} \tag{10}$$

where K, ΔT_{lm} and F are heat transfer coefficient, logarithmic mean temperature difference (LMTD), and correction coefficient, respectively. The parameter values are shown in Table **3**. ΔT_{lm} be calculated as:

$$\Delta T_{lm} = \frac{(T_{h,in} - T_{l,out}) - (T_{h,out} - T_{l,in})}{\ln \frac{(T_{h,in} - T_{h,out})}{(T_{l,out} - T_{l,in})}} \tag{11}$$

The annual operational cost A_c can be expressed as:

$$A_c = C_{OM} + EP \times E_{in} - R \tag{12}$$

where C_{OM} is the maintenance cost, Its value is set to 1.5% of the system's initial investment. EP represents the electricity price, and in this article, its value is 0.11 \$/kW·h, which R is the recovery value which value is 0 [23].

Table 2: The initial investment cost of each component [24, 25].

Components	Total Initial Investment Cost
Condenser, Evaporator	$1397 \times A^{0.89}$
Dual-function unit	$9624.2 \times W^{0.46}$
Circulating pump, Working fluid pump	$1129 \times W_p^{0.8}$
H-tank, L-tank	$280.3 \times q_m^{0.67}$
Throttle valve	$1120 \times q_m^{0.8}$

Table 3: Specific parameters of this proposed system.

Parameters	Meaning	Value
i	System life (y)	25
K_c	Total heat transfer coefficient [W/(m^2·K)]	1000
K_e		2500
F	Temperature difference correction factor	1

3.4. Boundary Conditions

For the established Carnot battery system, appropriate operating conditions are of paramount importance. This paper uses waste heat recovery as the heat source to provide thermal energy for the energy storage system. During the simulation, the heat source temperature is set to 80℃ and the upper storage temperature is the condensing temperature of the heat pump, considering the temperature rise capacity of the heat pump. Therefore, the upper storage temperature is set to 120℃. The storage temperature difference is set to 30℃, and the upper storage temperature is set to 90℃. The dual-function unit has both compression and expansion capabilities, with its compression efficiency and expansion efficiency set to 0.85 according to research literature [26]. The pinch temperature is necessary to ensure accurate stability during the heat exchange process, and it is assumed to be 5℃ in this paper. The cold source is derived from saturated water in the environment, with the cold source temperature set at 20℃. Table **4** lists the parameters of the settings above:

Table 4: Boundary parameters.

Parameters	Meaning	Value
$T_{sto,h}$	upper storage temperature [℃]	120
$T_{sto,l}$	lower storage temperature [℃]	90
$T_{hs,in}$	Heat source temperature [℃]	80
$T_{cond,orc}$	Condensing temperature of ORC [℃]	35
ΔT_{pp}	Pinch temperature of heat exchanger [℃]	5
ΔT_s	Superheat temperature [℃]	2
$\eta_{ise,hp}$	Isentropic efficiency of dual-function unit in HP mode	0.85
$\eta_{ise,orc}$	Isentropic efficiency of dual-function unit in ORC mode	0.85

4. Results and Discussion

The proposed Carnot battery system has been model-validated in Section 4.1. Subsequently, this paper conducts performance analysis and economic evaluation by changing pressure and temperature parameters in Sections 4.2 (discharge model) and Sections 4.3 (charge model). Finally, an exergy analysis of the components is carried out in Section 4.4, guiding future system optimization.

4.1. Model Validation

The current model is set to the same operating conditions as those of Rui Xia *et al*. [27] isentropic efficiencies of the expander and evaporator are 85%, the isentropic efficiency of the water pump is 80%, the ambient temperature is 10°C, and the ambient pressure is 101.325 kPa. The P2P variation of the Carnot battery system is observed by changing the heat source temperature. The data is obtained by "GetDate.exe", and the data point is the change of heat source temperature in P2P. After the above working state parameters are set, the heat source temperature is changed to compare the data of the two models to verify the accuracy of the model. The reference literature and simulation result data of this paper are shown in Fig. (**3**). It can be seen from the figure that the

maximum error between the two models reaches 5.2% when the heat source temperature is 75°C, proving the reliability of this model.
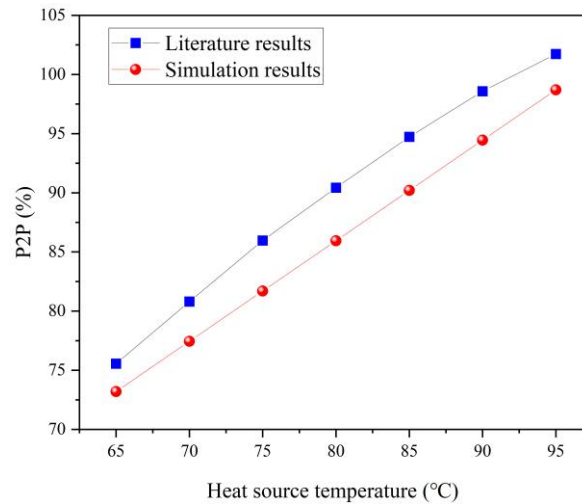

Figure 3: Simulation results and reference results.

4.2. Environmental Sensitivity Analysis

Fig. (**4**) delineates the sensitivity coefficients of P2P, LCOS, and exergy efficiency under the conditions of ambient temperature fluctuations. At an initial ambient temperature of 10℃, the optimal values for P2P, LCOS, and exergy efficiency are 52.61%, 0.42 $/kW·h, and 67.09%, respectively. The performance of the model deteriorates as the ambient temperature increases. When the ambient temperature rises by 15℃, the evaluated performance metrics reach 38.62, 0.53 $/kW·h, and 64.7%, respectively. Through sensitivity analysis, The P2P of this proposed system with its sensitivity coefficient decreasing by 60.38 is the most sensitive to the , with, indicating the most significant variation among the three. The exergy efficiency has the lowest sensitivity coefficient variation of 6.18.

The reason for this change is that the ambient temperature affects the condensation temperature in the ORC system. As the ambient temperature increases, the condensation temperature also increases. Under the constant conditions of $T_{sto,h}T_{sto,l}$ and, the decrease in the enthalpy drop of the expander working fluid leads to a reduction in W_{net}. According to equation 1, the thermoelectric conversion efficiency decreases, while the COP remains constant, ultimately resulting in a decrease in P2P.

The reduction W_{net} indirectly affects LCOS and exergy efficiency, according to equations 10-11. This leads to a relatively smaller change in the sensitivity coefficients of these two parameters compared to P2P.
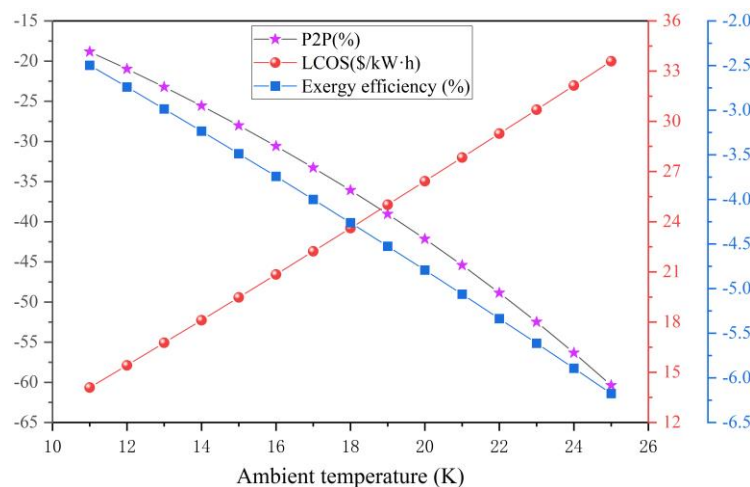

Figure 4: The sensitivity coefficient varies with changes in ambient temperature.

4.3. Performance Analysis Results

4.3.1. Discharge Mode

The system performance varies with pressure as shown in Fig. (**5**), where the horizontal axis represents the pressure drop at the expander inlet under the set reference points (upper thermal storage limit of 120°C and lower thermal storage limit of 90°C). As seen in Fig. (**5a**), the thermoelectric conversion efficiency decreases from 5.99 % to 5.82 % as the pressure drops from 1 kPa to 15 kPa. The enthalpy of the gas entering the expander decreases with the decrease in pressure, and the outlet parameters set for the expander remain unchanged, resulting in a reduction of the kinetic energy obtained by the expander. However, the heat absorbed by the gas from the evaporator remains constant. According to Equation 1, the thermoelectric conversion efficiency decreases. The pressure drop variation at the ORC system expander does not affect the HP system parameters, resulting in a constant COP, and the P2P changes in tandem with the thermoelectric conversion efficiency, decreasing from 26.97% to 26.2%.

According to Fig. (**5b**), as the pressure drop increases from 1 kPa to 15 kPa, the LCOS rises from 0.65 $/kW·h to 0.66 $/kW·h. Based on the aforementioned analysis, the system output power decreases (output power changes from 14.9 kW to 14. 5 kW) while the input energy remains unchanged, resulting in an increase in cost and a higher LCOS. Simultaneously, the overall efficiency also decreases correspondingly, reaching a minimum of 62.8%.
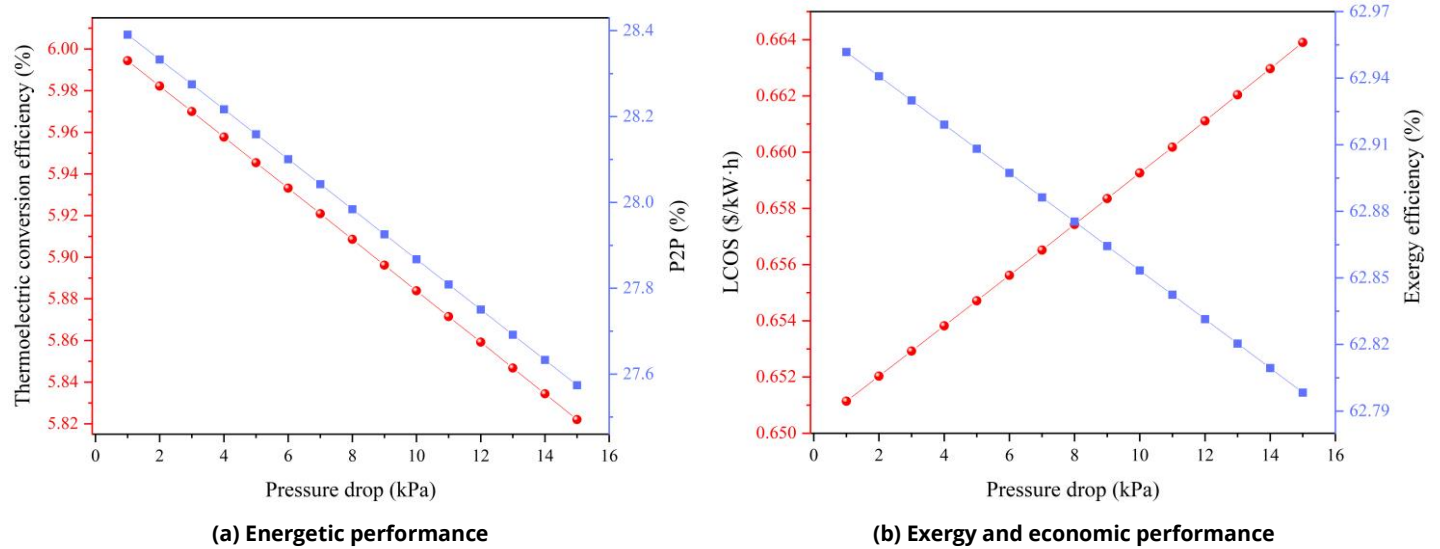

(a) Energetic performance   (b) Exergy and economic performance

Figure 5: Variation of system performance with the pressure drop.

The system performance exhibits an increase with temperature as illustrated in Fig. (**6**). According to Fig. (**6a**), the COP remains constant at 4.74, and the thermal conversion efficiency increases, reaching a maximum of 13.02% at a temperature rise of 15°C. This can be explained as follows: as the inlet temperature of the expander increases, the enthalpy drop per unit of working fluid becomes larger due to the constant outlet parameters of the expander. Based on Equation 1, the thermoelectric conversion efficiency increases.

In Fig. (**6b**), the overall exergy efficiency of the system increases from 63.38% to 69.02% with the temperature rise. Meanwhile, the LCOS, which characterizes the economic performance, changes from 0.62 $/kW·h to 0.37 $/kW·h, and the rate of change gradually slows down. The main reason for this effect is due to the increase in both parameter E_{out} and annual operating costs with the temperature rise. The parameter increases from 7.26*E6 kWh to 12.28*E6 kWh, with a growth rate of 69.14%, and the annual operating costs increase from 0.71 M$/kW·h to 1.07 M$/kW·h, with a growth rate of 50.7%. Since the increase in the parameter E_{out} is slower than the annual operating costs, according to Equation 11, the rate of increase in LCOS slows down.

As the inlet temperature of the expander increases, it leads to improved thermal conversion efficiency and LCOS; however, there must be sacrifices in other aspects of performance. Fig. (**6c**) illustrates this effect. The exergy

loss of the evaporator component gradually increases with the temperature rise, reaching a maximum of 23.6 kW, accompanied by a gradual decrease in exergy efficiency (from 71.4% to 66.2%). The temperature rise causes an increase in the temperature difference between the heat exchange fluids in the evaporator, leading to higher irreversible losses and a decrease in power efficiency.
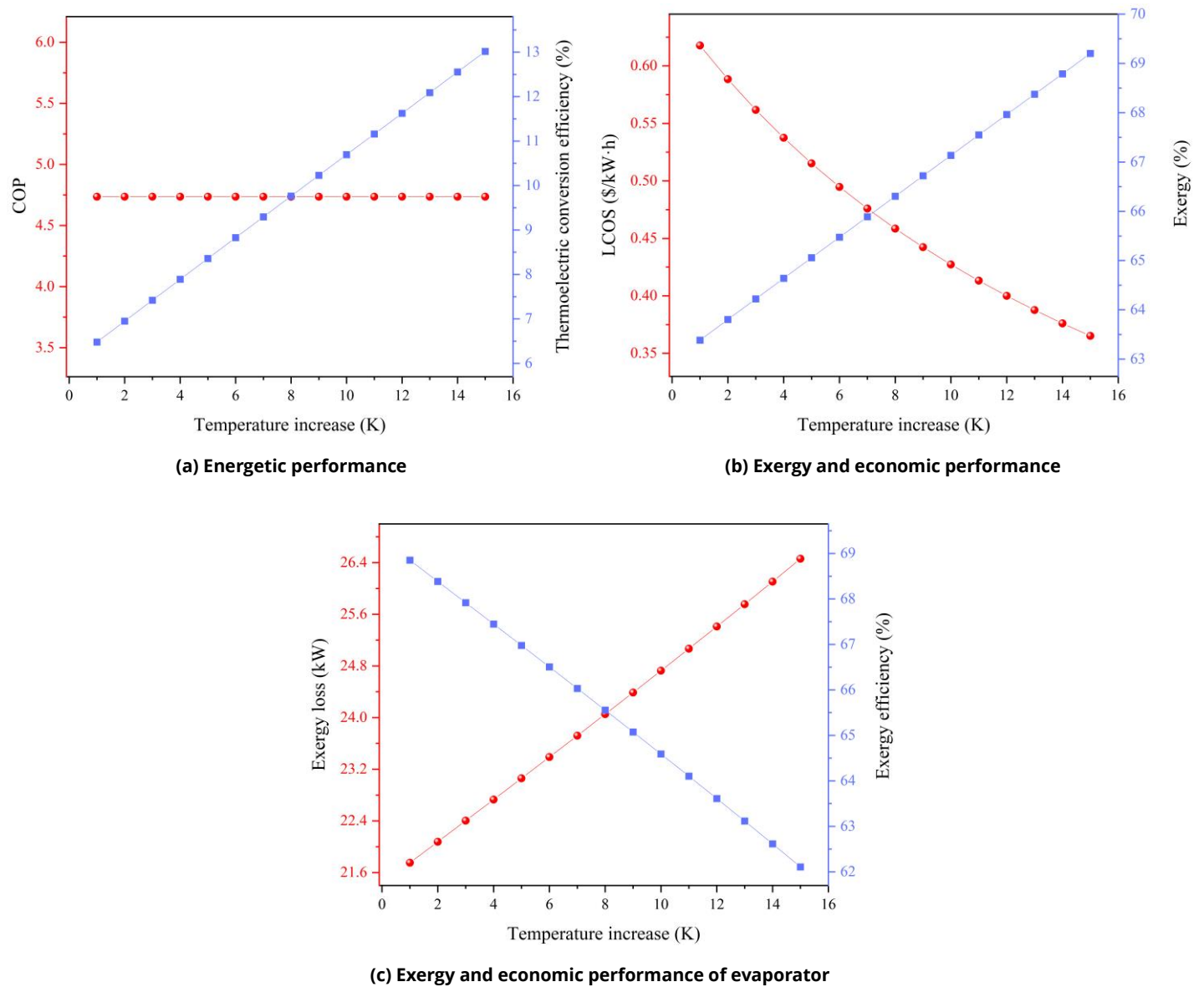
(a) Energetic performance

(b) Exergy and economic performance

(c) Exergy and economic performance of evaporator

Figure 6: Variation of system performance with the temperature increase.

4.3.2. Charging Mode

In the charging mode, Fig. (**7**) demonstrates the performance of the Carnot battery system as the pressure drop changes. According to Fig. (**7a**) and Fig. (**7b**), the system's thermodynamic performance worsens with decreasing pressure, with the maximum P2P and exergy efficiency reaching 25.04% and 61.82%, respectively. As previously mentioned, the reduction in pressure leads to lower enthalpy values, while the enthalpy of the gas at the outlet of the dual-function unit remains unchanged. This results in the working fluid being able to absorb more heat before and after compression, but the corresponding input power will increase. According to the simulation values, the input power increases from 70.22 kW to 71.82 kW, while the heat obtained from the heat source remains constant, leading to a decline in performance.
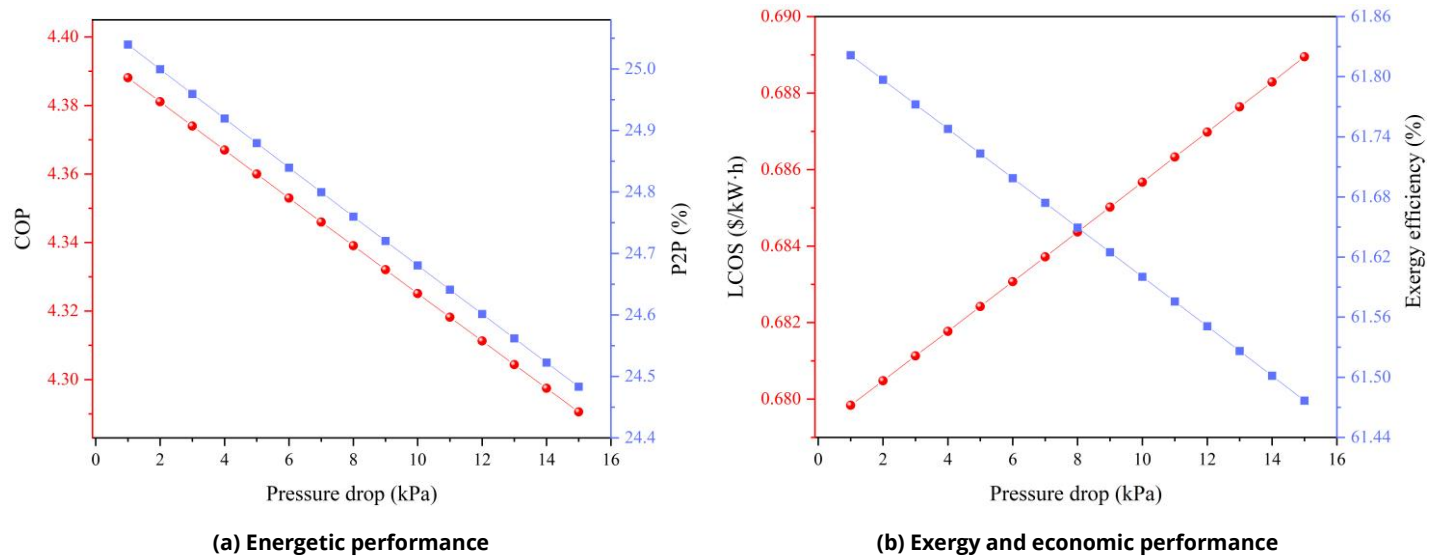
(a) Energetic performance   (b) Exergy and economic performance

Figure 7: Variation of system performance with the pressure drop.

The influence of temperature rise on the Carnot battery system in charging mode is depicted in Fig. (**8**). As the temperature rise gradually increases, the thermoelectric conversion efficiency remains constant at 6% according to Fig. (**8a**), while the COP gradually increases at an accelerating rate. During the temperature change process, the heat exchange of the condenser component remains unchanged, with xxx maintaining a constant value of 261.9 kW. Due to the increased temperature, the enthalpy of the gas at the inlet of the dual-function unit increases, while the outlet working fluid enthalpy remains unchanged, and the compression power correspondingly decreases linearly, with the lowest value being 27.27 kW. Thus, the COP exhibits the depicted change according to equation 3. As shown in Fig. (**8b**), the economic and power performance of the Carnot battery system also improves correspondingly, reaching their optimum values of 0.41 \$/kW·h and 73.38% at a temperature rise of 15℃.
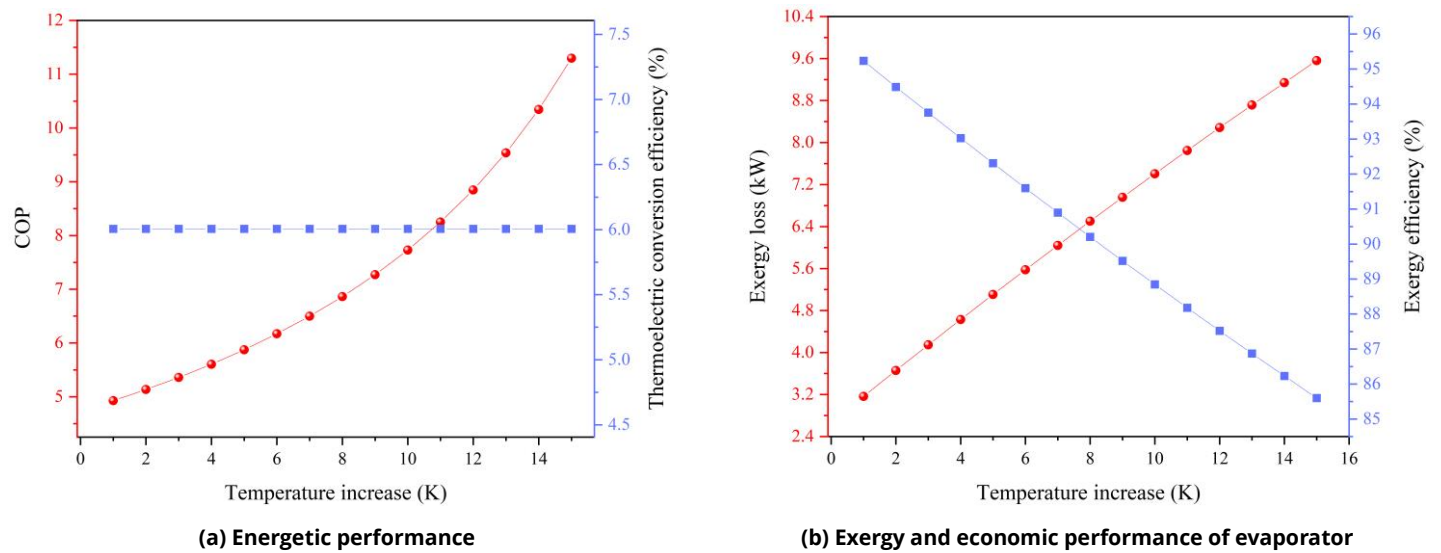

(a) Energetic performance   (b) Exergy and economic performance of evaporator

Figure 8: Variation of system performance with the temperature increase.

4.4. Exergy Loss Analysis

Exergy can evaluate energy from a quality perspective, and exergy loss analysis can determine the energy quality loss in the energy conversion process of equipment. Fig. (**9**) shows the exergy loss performance of the Carnot system in discharge mode under the set parameters. According to Fig. (**9**), the component with the largest exergy loss is the evaporator, with a maximum exergy loss of 21.16 kW, accounting for 40.1% of the total exergy

loss in the discharge mode. At the same time, the evaporator has the highest exergy efficiency, reaching 69.32%. The evaporator generates exergy loss due to irreversible losses caused by temperature differences and undergoes a large amount of heat exchange (258.7 kW), far exceeding other components. Even with a relatively high exergy efficiency, the evaporator still has a significant exergy loss. The condenser has an exergy loss of 9.91 kW and the lowest exergy efficiency, which is caused by the large temperature difference at both ends of the heat exchange fluid on the condenser side. The exergy loss during the charging process can be seen in Fig. (**10**). The condenser has the lowest performance: the largest exergy loss (38.06 kW) and the lowest exergy efficiency (64.43%). The evaporator has the lowest exergy efficiency and ranks second in exergy loss. The evaporator has an exergy efficiency of only 64.43%, and its exergy loss is 38.64 kW, ranking second.
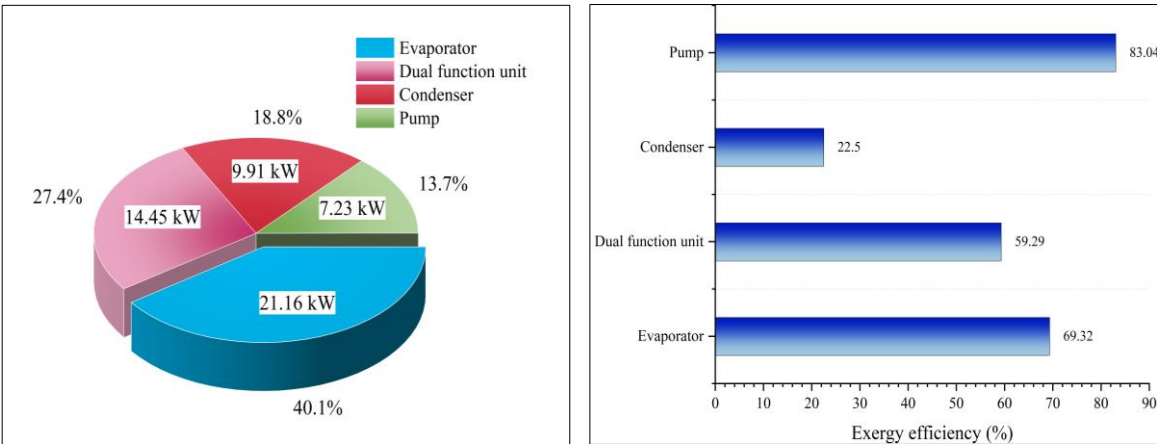

Figure 9: Exergy performance of the Carnot battery system in the discharging mode.

From the above analysis, it can be concluded that improving the evaporator and condenser of the Carnot battery can optimize the exergy performance. The main approach is to reduce the irreversible losses in the heat exchange process by minimizing the temperature difference. However, this leads to an increase in the heat exchanger area, resulting in a cost increase according to Equation 13.
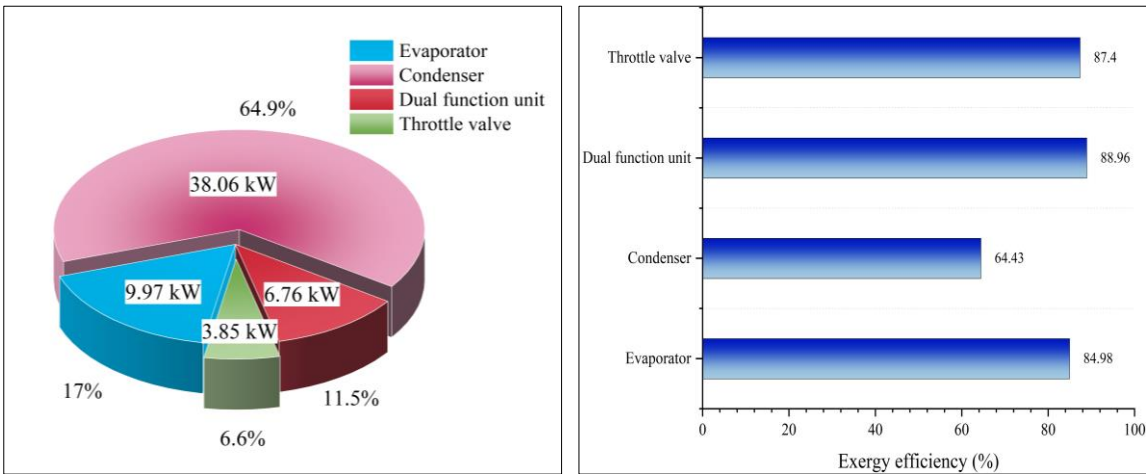

Figure 10: Exergy performance of the Carnot battery system in the charging mode.

4.5. Heat Exchangers Analysis

The LMTD of the heat exchanger can notably sway the size of the heat exchanger, thereby influencing the annual operating cost. The discussion about the LMTD of the heat exchanger proves beneficial when conducting a comprehensive assessment of the heat exchanger's performance.

The diminution of exergy loss with the decrease in LMDT is depicted in Fig. (**11**). The minimum exergy loss in the evaporator can be reduced to 14.35 kW when its LMDT is 2.39, while the minimum exergy loss in the condenser can be reduced to 22.93 kW when its LMDT is 1.86. When the LMDT in the evaporator and condenser are identical, it can be observed that the exergy loss in the condenser is greater, attributable to its larger heat exchange capacity.
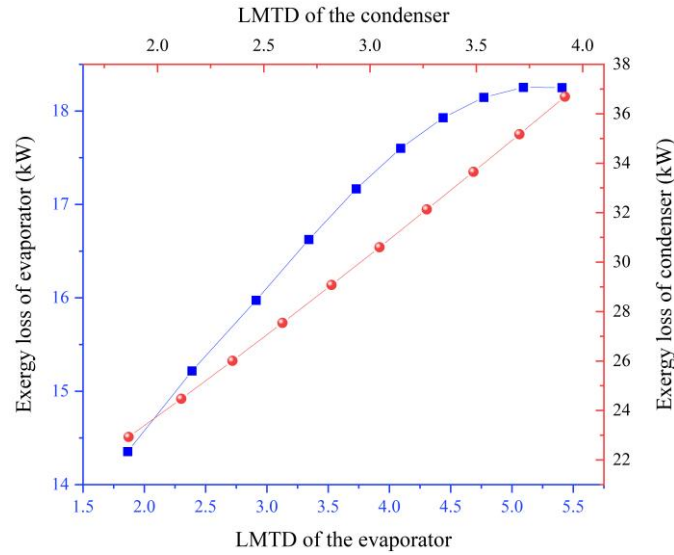

Figure 11: Exergy loss under various LMTD.

As illustrated in Fig. (**12a**), the surface area of the evaporator decreases concomitant with an increase in LMTD, reaching its nadir of 5.18 at an LMTD of 5.41. From Fig. (**12a**), it is identifiable that its rate of reduction progressively dwindles. This results from variations in the heat source side temperature, discussed in the modeling, that do not impact the working fluid side temperature. Throughout the process wherein the LMTD gradually lessens, it changes from 5.41 to 2.39 - a rate alteration of 55.82%. The logarithmic relationship contributes to a smaller reduction in the quantity of heat source side temperature difference. The heat dissipation of the heat source drops from 798 kW to 420 kW, a reduction of 46.24%. According to Equation 13, the rate at which the heat exchange surface area of the evaporator grows diminishes.

The reduction in the evaporator area results in the initial investment of the evaporator decreasing from 0.55 M$/kWh to 0.33 M$/kWh. Concurrently, due to the diminution of the heat source dissipation, the surface area of the condenser also decreases under the condition of a consistent condenser LMTD, thereby reducing the initial investment (from 2.29 M$/kWh to 1.4 M$/kWh). Ultimately, this culminates in a decrease in the LCOS.

According to the above model setting conditions, increase with the rise in the heat source outlet temperature. Exergy efficiency increases and the maximum value is 61.33% when LMTD is 2.39 according to Equation 10.
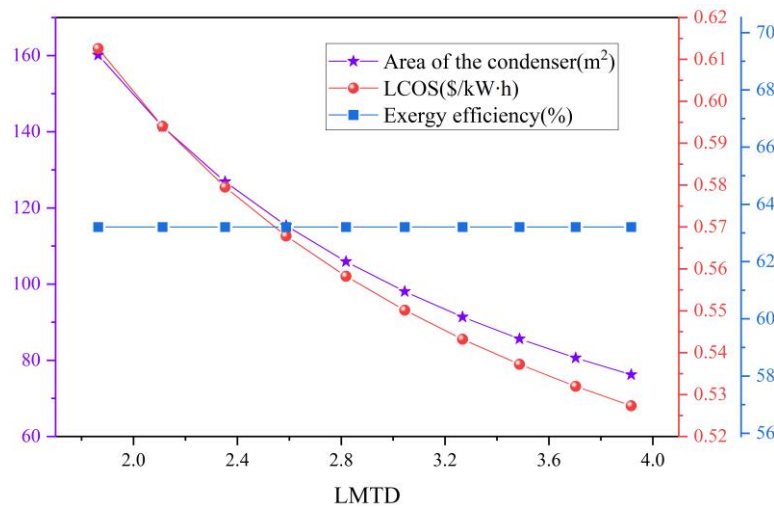
The performance of the condenser varies with its LMTD as shown in Fig. (**12b**). The condenser area and condenser exergy efficiency have a similar trend compared with the evaporator. The difference is that the condenser efficiency does not change to 63.21%. Modifying the upper and lower temperature limits in the model setup does not affect the exergy efficiency according to Equation 10.

5. Conclusion

This paper conducts a non-saturated analysis of the proposed Carnot battery energy storage system. By changing the inlet temperature and pressure parameters of the dual-function unit, it is transformed into a non-saturated state, and a thermodynamic and economic analysis of the system is performed. Under the set state parameters, the exergy analysis is carried out. The performance of the evaporator and condenser under different logarithmic mean temperature differences is explored, and the Carnot battery energy storage system is evaluated comprehensively:
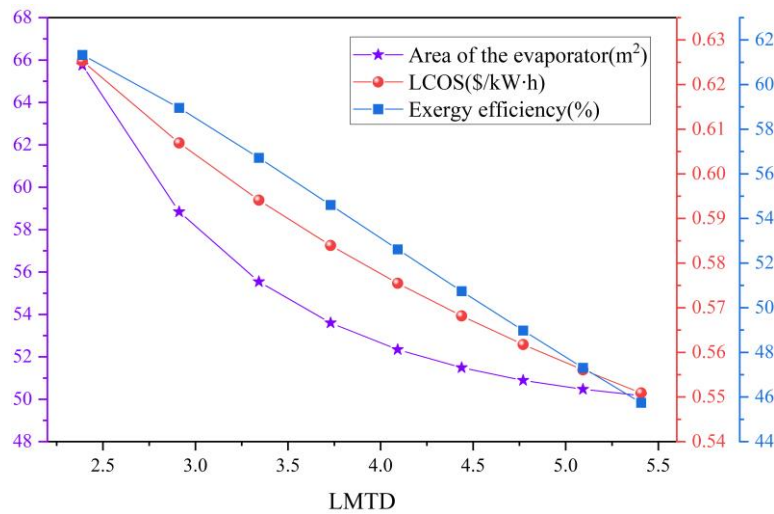
(a)

(b)

Figure 12: Performance of evaporator (**a**) and condenser (**b**) under various LMTD.

(1) The performance of the model deteriorates as the ambient temperature increases. The optimal values for P2P, LCOS, and exergy efficiency are respectively 61.82%, 0.42 $/kW·h, and 67.09% at a temperature of 10℃. P2P demonstrates the greatest sensitivity, with its coefficient decreasing by 60.38 through sensitivity analysis.

(2) Pressure drop is unfavorable for economic and thermodynamic performance, and has a significant impact on the charging system. When the pressure drop in the charging mode is 15 kPa, the Carnot battery system's P2P, LCOS, and exergy efficiency can reach 25.77%, 0.65 $/kW·h, and 67.09%.

(3) Temperature rise is beneficial for improving the thermodynamic and economic performance of the Carnot battery system. When the temperature rise is 15℃, the optimal P2P, LCOS, and exergy efficiency of the Carnot battery system can reach 67.86%, 0.43 $/kW·h, and 72.81%.

(4) The evaporator and condenser have the largest exergy losses and need optimization. In the discharge mode, the component with the highest exergy loss is the evaporator, with a maximum exergy loss of 21.16 kW and the highest exergy efficiency reaching 69.32%. In the charging mode, the condenser has the lowest performance: the highest exergy loss (38.06 kW) and the lowest exergy efficiency (64.43%).

(5)   A diminution of the LMTD within the evaporator catalyzes an augmentation in the LCOS and a concurrent decline in the exergy efficiency. The optimum recorded LCOS value is 0.55 $/kW·h, and an exergy efficiency of 61.33% is observed at LMTD values of 5.41 and 2.39 respectively. Variations in the LMTD of the condenser do not incite changes in the exergy efficiency, which consistently maintains at a steady 63.21%.

Conflict of Interest

The authors declare that they have no known competing financial interests or personal relationships that could have appeared to influence the work reported in this paper.

Funding

References

[1]   Ge X, Ma Y, Li Y, Jiao Y, Wang Z, Wu F, et al. Daily peak shaving operation of mixed pumped-storage hydro plants considering cascade hydraulic coupling. Energy Rep. 2023; 9: 971-8. https://doi.org/10.1016/j.egyr.2023.05.207

[2]   Efkarpidis NA, Imoscopi S, Geidl M, Cini A, Lukovic S, Alippi C, et al. Peak shaving in distribution networks using stationary energy storage systems: A Swiss case study. Sustain Energy Grid Netw. 2023; 34: 101018. https://doi.org/10.1016/j.segan.2023.101018

[3]   Meng Y, Cao Y, Li J, Liu C, Li J, Wang Q, et al. The real cost of deep peak shaving for renewable energy accommodation in coal-fired power plants: Calculation framework and case study in China. J Clean Prod. 2022; 367: 132913. https://doi.org/10.1016/j.jclepro.2022.132913

[4]   Zhang M, Shi L, Zhang Y, He J, Sun X, Hu P, et al. Configuration mapping of thermally integrated pumped thermal energy storage system. Energy Convers Manag. 2023; 294: 117561. https://doi.org/10.1016/j.enconman.2023.117561

[5]   Sharma S, Mortazavi M. Pumped thermal energy storage: A review. Int J Heat Mass Transf. 2023; 213: 124286. https://doi.org/10.1016/j.ijheatmasstransfer.2023.124286

[6]   Sorknæs P, Thellufsen JZ, Knobloch K, Engelbrecht K, Yuan M. Economic potentials of carnot batteries in 100% renewable energy systems. Energy. 2023; 282: 128837. https://doi.org/10.1016/j.energy.2023.128837

[7]   Su Z, Yang L, Song J, Jin X, Wu X, Li X. Multi-dimensional comparison and multi-objective optimization of geothermal-assisted Carnot battery for photovoltaic load shifting. Energy Convers Manag. 2023; 289: 117156. https://doi.org/10.1016/j.enconman.2023.117156

[8]   Niu J, Wang J, Liu X, Dong L. Optimal integration of solar collectors to Carnot battery system with regenerators. Energy Convers Manag 2023; 277: 116625. https://doi.org/10.1016/j.enconman.2022.116625

[9]   Canpolat Tosun D, Açıkkalp E, Altuntas O, Hepbasli A, Palmero-Marrero AI, Borge-Diez D. Dynamic performance and sustainability assessment of a PV driven carnot battery. Energy. 2023; 278: 127769. https://doi.org/10.1016/j.energy.2023.127769

[10]   Hu S, Yang Z, Li J, Duan Y. Thermo-economic analysis of the pumped thermal energy storage with thermal integration in different application scenarios. Energy Convers Manag. 2021; 236: 114072. https://doi.org/10.1016/j.enconman.2021.114072

[11]   Dai R, Tian R, Zheng S, Wei M. Finite-time thermodynamic and economic analysis of Rankine Carnot battery based on life-cycle method. Appl Therm Eng. 2023; 230: 120813. https://doi.org/10.1016/j.applthermaleng.2023.120813

[12]   Fan R, Xi H. Energy, exergy, economic (3E) analysis, optimization and comparison of different Carnot battery systems for energy storage. Energy Convers Manag. 2022; 252: 115037. https://doi.org/10.1016/j.enconman.2021.115037

[13]   Ma R, Qiao H, Yu X, Yang B, Yang H. Thermo-economic analysis and multi-objective optimization of a reversible heat pump-organic Rankine cycle power system for energy storage. Appl Therm Eng. 2023; 220: 119658. https://doi.org/10.1016/j.applthermaleng.2022.119658

[14]   Steger D, Regensburger C, Eppinger B, Will S, Karl J, Schlücker E. Design aspects of a reversible heat pump - Organic rankine cycle pilot plant for energy storage. Energy. 2020; 208: 118216. https://doi.org/10.1016/j.energy.2020.118216

[15]   Mosaffa AH, Farshi LG, Infante Ferreira CA, Rosen MA. Exergoeconomic and environmental analyses of CO2/NH3 cascade refrigeration systems equipped with different types of flash tank intercoolers. Energy Convers Manag. 2016; 117: 442-53. https://doi.org/10.1016/j.enconman.2016.03.053

[16]   Ahmadi MH, Sayyaadi H, Mohammadi AH, Barranco-Jimenez MA. Thermo-economic multi-objective optimization of solar dish-Stirling engine by implementing evolutionary algorithm. Energy Convers Manag. 2013; 73: 370-80. https://doi.org/10.1016/j.enconman.2013.05.031

[17]   Martínez de León C, Ríos C, Molina P, Brey JJ. Levelized Cost of Storage (LCOS) for a hydrogen system. Int J Hydrogen Energy. 2023 (in press). https://doi.org/10.1016/j.ijhydene.2023.07.239

[18]   Wang L, Lin X, Zhang H, Peng L, Zhang X, Chen H. Analytic optimization of Joule–Brayton cycle-based pumped thermal electricity storage system. J Energy Storage. 2022; 47: 103663. https://doi.org/10.1016/j.est.2021.103663

[19]   Berstad D, Gundersen T. On the exergy efficiency of CO2 capture: The relation between sub-process and overall efficiencies. Carbon Capture Sci Technol. 2023; 7: 100111. https://doi.org/10.1016/j.ccst.2023.100111

[20]   Kirtania B, Shilapuram V. Conceptual design, energy, exergy, economic and water footprint analysis of CO2-ORC integrated dry gasification oxy-combustion power cycle. J Clean Prod. 2023; 416: 137930. https://doi.org/10.1016/j.jclepro.2023.137930

[21]   Yu X, Li Z, Zhang Z, Wang L, Qian G, Huang R, *et al*. Energy, exergy, economic performance investigation and multi-objective optimization of reversible heat pump-organic Rankine cycle integrating with thermal energy storage. Case Stud Thermal Eng. 2022;38: 102321. https://doi.org/10.1016/j.csite.2022.102321

[22]   Yu X, Qiao H, Yang B, Zhang H. Thermal-economic and sensitivity analysis of different Rankine-based Carnot battery configurations for energy storage. Energy Convers Manag. 2023; 283: 116959. https://doi.org/10.1016/j.enconman.2023.116959

[23]   Xu G, Liang F, Yang Y, Hu Y, Zhang K, Liu W. An improved CO2 separation and purification system based on cryogenic separation and distillation theory. Energies. 2014; 7: 3484-502. https://doi.org/10.3390/en7053484

[24]   Sanaye S, Shirazi A. Four E analysis and multi-objective optimization of an ice thermal energy storage for air-conditioning applications. Int J Refrig. 2013; 36: 828-41. https://doi.org/10.1016/j.ijrefrig.2012.10.014

[25]   Babajamali Z, khabaz MK, Aghadavoudi F, Farhatnia F, Eftekhari SA, Toghraie D. Pareto multi-objective optimization of tandem cold rolling settings for reductions and inter stand tensions using NSGA-II. ISA Trans. 2022; 130: 399-408. https://doi.org/10.1016/j.isatra.2022.04.002

[26]   Xia R, Wang Z, Cao M, Jiang Y, Tang H, Ji Y, *et al*. Comprehensive performance analysis of cold storage Rankine Carnot batteries: Energy, exergy, economic, and environmental perspectives. Energy Convers Manag. 2023; 293: 117485. https://doi.org/10.1016/j.enconman.2023.117485

[27]   Lei K, Chang J, Wang X, Guo A, Wang Y, Ren C. Peak shaving and short-term economic operation of hydro-wind-PV hybrid system considering the uncertainty of wind and PV power. Renew Energy. 2023; 215: 118903. https://doi.org/10.1016/j.renene.2023.118903